Original Research

Adsorption of Antimony(III) onto Fe(III)-Treated Humus Sludge Adsorbent: Behavior and Mechanism Insights

Ren-Jian Deng[1-3]*, Rang Shao[1], Bo-Zhi Ren[1], Baolin Hou[1], Zhi-E Tang[1], Andrew Hursthouse [1]

[1]School of Civil Engineering, Hunan University of Science and Technology, Xiangtan, China
[2]School of Resource Environment and Safety Engineering, Hunan University of Science and Technology, Xiangtan, China
[3]Hunan Jing Yi Environmental Protection High Tech Development Co. Ltd., Xiangtan, China

Abstract

In this study, adsorption behaviors and mechanisms of Sb(III) ions onto Fe(III)-treated humus sludge adsorbent (FTHSA) from aqueous solutions was investigated using batch adsorption techniques, Fourier transform infrared (FT-IR) spectra and scanning electron microscopy were coupled to an energy-dispersive spectrometer (EDS). FTHSA was prepared via immersion with 1 mol/L FeCl$_3$. The effects of dosage, contact time, Sb(III) initial concentration, and pH on the adsorption of Sb(III) onto FTHSA were investigated. Sb(III) adsorption was favored at pH with 2.0 and decreased dramatically with increasing pH. The description of equilibrium data of Sb(III) adsorption by Langmuir, Freundlich, and Dubbin-Radushkevich isotherm models showed that Langmuir model provided the best fit for Sb(III) adsorption with maximum adsorption amount of 9.433 mg/g. Pseudo first-order, pseudo second-order, Elovich, and intraparticle diffusion model were applied to describe the adsorption process of Sb(III) ions onto FTHSA. The results showed that the pseudo second-order model described well how Sb(III) adsorption and chemical adsorption played a dominant role in the adsorption process. The FT-IR spectra also indicated that the chemical interactions as ion exchange among the metal ions and N-H, O-H, C=O, COO, and C-O were mainly involved in the adsorption process. Therefore, FTHSA has a suitable potential removal for Sb(III) ions in the practical process.

Keywords: antimony (III), humus sludge adsorbent, Fe(III)-treated, adsorption isotherm, kinetic model

---

*e-mail: 800912deng @sina.com

Introduction

Antimony (Sb) is mainly found in only oxidation states (III, V) at pH of 2~10 in natural water environment [1]. Human exposure to Sb is primarily accumulated through drinking water and the food chain, causing damage to the liver, lungs, and cardiovascular system [2]. Sb and its compounds have far-reaching impacts because of its strong mobility and complexation reactions in the environment [3], and are considered global pollutants and priority control pollutants by many countries or regions [4]. However, Sb is widely used in various industries such as alloys, glasses, plastics, and batteries, making waste incineration an important source of Sb to the water environment [5]. China is the largest Sb producer in the world with approximately 90% of the world's production [6]. Due to the complex characteristics of wastewater containing antimony, the lack of latest technology and chaotic management, etc., many surface and ground waters are seriously polluted by the Sb-containing wastewater with large discharge standard in China [7-8]. Therefore, Sb poisoning and pollution events should concern scientists in China.

Some treatment methods for Sb have been developed in the past few decades, such as coagulation precipitation, the biological method, and adsorption and electrochemical methods, etc. [4]. Among them, biosorbents in the genre of Lichens [9], cyanobacteria [10], seaweed [11], sludge [12-13] and other waste materials have performed well in the sequestration of Sb ions from aqueous solutions. Owing to the advantages of large adsorption capacity, low cost, and being widely sourced, the sludge adsorbents that contain carboxyl, amino, hydroxyl, and phosphoric acid groups are applied to removal harmful heavy metals ions from solution by some researchers [14-15]. Meanwhile, granulation and modification technologies were be developed for overcoming the shortcomings of the poor separation of muddy and water and the low adsorption capacity [4, 16-17]. Moreover, Fe(III) modification technology is considered to be one of the best modifications and strengthening technologies for Sb removal [12-13, 18]. However, humus sludge and Fe(III)-modification technology for removing antimony is rarely reported. So, influencing factors and adsorption mechanisms are not clear and need to be further studied.

The aims of this paper are to: (1) prepare Fe(III)-treated humus sludge adsorbent (FTHSA), (2) characterize the structural and surface characteristics of FTHSA by Fourier transmission infrared spectroscopy (FT-IR) and scanning electron microscope (SEM), and (3) survey the influence factors, adsorption isotherm, and kinetics consequence of Sb(III) iron onto FTHSA by using batch equilibration method. The results of this paper may provide theoretical and technical support for the treatment of antimony-containing wastewater.

Material and Methods

Humus Sludge and FTHSA

Fresh sludge was collected from Xiangtan Wastewater Treatment Plant in Hunan Province. The main character of the sludge included moisture content 76%, pH value 6.8, and volatile suspended solids 45.8%. About 10 kg fresh sludge was dried in a freeze drier at 105ºC again to a constant weight, then ground and sieved (100 mesh). The fresh sludge adsorbent appeared in the form of fine powder and was stocked before use. According to the literature [14], the other 10 kg sludge was fermented in the conditions of aerobic ventilation for 35 days. Then, as in previous examples, the humus sludge sorbent appeared and was stocked in a desiccator before use. According to reference [12], 50 g humus fine powder was added to 500 ml and 1 mol L^{-1} $FeCl_3$ solution. Under continuous shaking at 100 rpm for 24 h, the humus fine powder was collected and washed repeatedly by deionized water until no Fe(III) ions were detected in the supernatant. The suspension was filtrated and dried in a freeze drier at 80ºC again to a constant weight. The FTHSA appeared in the form of fine powder and was stocked in a desiccator before use.

Chemicals

Potassium antimony tartrate (purity>99.9%), $NaBH_4$, NaOH, KI, ascorbic acid, etc., with a purity of 99.0% were purchased from Flying Boat Chemical Reagents Technology Co. Ltd. Tianjin, China. HCl purchased from Beijing Chemical Industry Co., Ltd, was excellent grade pure. The experimental water was taken from Synergy UV Millipore water (Millipore, USA). Configured Sb(III) aqueous solutions of 25 mg L^{-1} concentrations were stored in a refrigerator at 4ºC.

Batch Sorption Procedure

Sorption experiments were performed by batch equilibrium method. Some FTHSA was mixed with 250 ml of 25 mg L^{-1} Sb(III) solution at 25ºC. Upon reaching the adsorption equilibrium, the formed suspension was continuously stirred at the stirring rate of 3000 rpm for 5 mins. The above supernatant was then filtered with a 0.45 μm pore-size cellulose acetate membrane filter. Some part of filtrated aliquot was used to analyze the residual Sb(III) concentrations. The other was used to determine the final pH. All experiments were performed in triplicate. The adsorption experiment was carried out under sealed light conditions.

At the conditions of pH 6.0, dosage of 4.2 g L^{-1}, reaction time of 120 min, and Sb(III) initial concentration of 25 mg L^{-1}, the experiments were carried out to investigate the adsorption differences of sludge adsorbents, humus sludge adsorbents, and FTHSA. Then, the effects of pH (1~6), adsorbent dosage (1~6 g L^{-1}), Sb(III) initial concentration (10~450 mg L^{-1}),

and temperature (10~30ºC) on the removal of antimony by FTHSA were investigated by a single factor test. The isothermal adsorption experiment was carried out at pH = 2 and the adsorption isotherm concentration range was 10.0~450.0 mg L^{-1}. The adsorption kinetics experiments lasted 400 min, and sampling at different time intervals to analyze the concentration of supernatant concentration Sb(III).

The adsorption removal rate is calculated as follows [12]:

$$Biosorption(\%) = \frac{C_i - C_f}{C_i} \times 100\%$$ (1)

…where C_i and C_f (mg L^{-1}) are the initial and equilibrium concentrations of Sb(III) in solution, respectively.

Characterization and Analytical Methods

The concentration of Sb(III) in the experiment was determined by an AFS-9700atomic fluorescence spectrophotometer. Separating Sb(III) and Sb(V) with a strong anion exchange column (PRP X100), the ammonium tartrate (200.0 mmol L^{-1}, pH 5) was liquid. The system can do morphological analysis with Sb(III) and Sb(V) while achieving detection. The sample was tested at the same time as a blank test to replace the sample with deionized water. The recycling of Sb(III) was calculated to be 90.0%-99.5%. Sb(V) was not detected, implying that Sb(III) did not trigger an oxidation reaction during the adsorption process.

The interface interactions of humus sludge sorbent, and FTHSA and FTHSA adsorption of Sb(III) were investigated using SEM-EDS and FT-IR. All of the lyophilized samples were sprayed with gold and analyzed by SEM (JSM-6380LV, Japanese electronics company) coupled with EDS spectroscopy (Bruker XFlash 5010, Germany). The FT-IR spectra were investigated using a Niclet 6700 spectrometer.

Results and Discussion

Effect of Sludge Types

As shown in Fig. 1, the highlighted variation of the adsorbed onto three adsorbents with the adsorption removal rate of Sb(III) 47.72%, 63.21%, and 86.51%, respectively. The results indicated that both humus treatment and Fe(III)-modification could improve the adsorptive removal of Sb(III). Compared with humus sludge, the FTHSA presented better adsorption performance. This was consistent with the experimental results by Wu et al. [10]. According to the modification data (data not shown), 1 mol L^{-1} Fe(III) was selected as an optimal pretreatment.
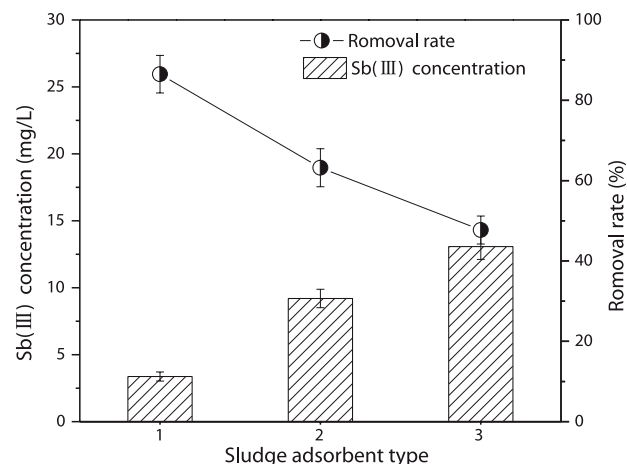

Fig. 1. Effect of Sludge types (1: FTHSA, 2: humus sludge, 3: Fresh sludge) on the removal rate of Sb(III) ions.

Effect of pH

Effects of pH on the removal rate of Sb(III) ions by FTHSA are displayed in Fig. 2. At pH in the range of 1~6, the removal rate increased first and then decreased, and the highest removal rate of 89.00% was reached at pH = 2. The removal rate displayed no significant changes with pH in the range of 2~4, which is close to the other observed results by Kumar B, et al. [12, 19]. But it's less than the acidity coefficient pKa (3.6) of antimony potassium tartrate, which may be related to Fe(III)-modification. The presence of Sb in solution is very complex and closely related to pH value. When pH<2, Sb(III) is mainly cationic Sb(OH)$^{2+}$, in the range of 2~10.7, it is mainly composed of H$_3$SbO$_3$ [4]. According to the calculating software Visual MINTEQ, at 20ºC antimony potassium tartrate exists in a variety of forms. With pH of 2~3, in the form of Sb(OH)$_3$ it accounted for
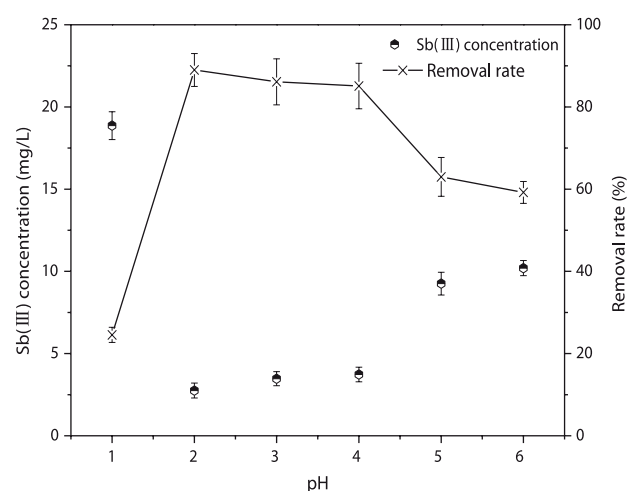

Fig. 2. Effects of pH on the removal rate of Sb(III) ions by FTHSA: Initial concentration of Sb(III) = 25 mg L^{-1}, contact time = 120 min, temperature = 20ºC, dosage of sorbent = 4.2 g L^{-1}, and volume of solution = 250 mL.
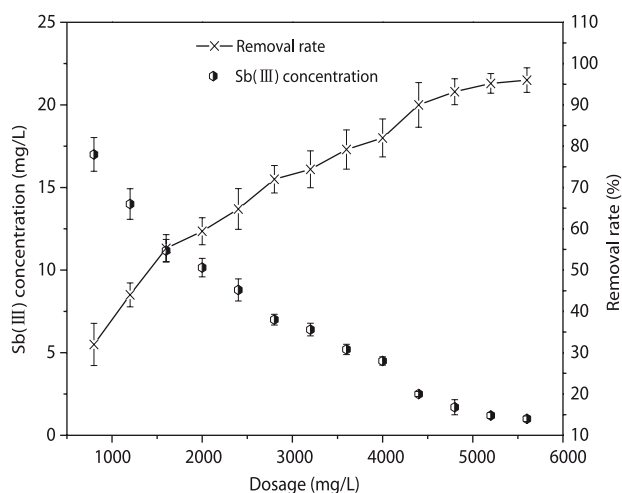
Fig. 3. Effects of dosage on the removal rate of Sb(III) ions by FTHSA: pH = 5, initial concentration of Sb(III) = 25 mg L^{-1}, contact time = 60 min, temperature = 20ºC, volume of solution = 250 mL.
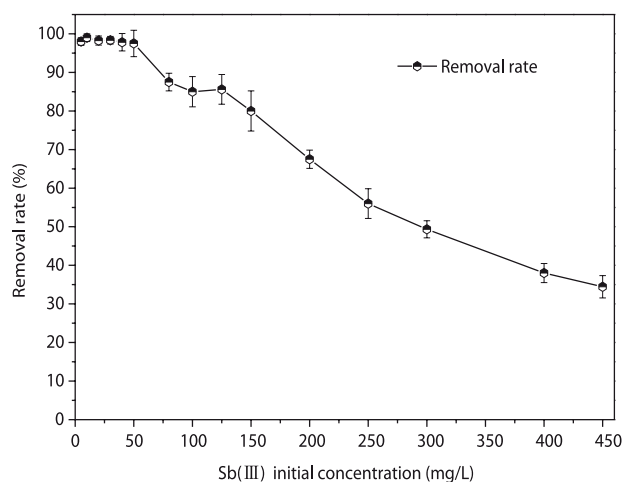

Fig. 4. Effects of initial concentration on the removal rate of Sb(III) ions by FTHSA: Contact time = 60 min, pH = 2, temperature = 20ºC, dosage of sorbent = 4.2 g L^{-1}, volume of solution = 250 mL.

75%~80.0% , the rest is the Sb(OH)$^{2+}$ or SbO$^+$ [20]. And with pH of 4~7, Sb(OH)$_3$ accounts for 99.0% or more. When pH<2, H$^+$ will completely combine with Sb(OH)$^{2+}$ for adsorption sites, and the increase of pH will inhibit the formation of Fe(III) hydroxyl iron oxide and the solubility of iron ion, which will reduce the adsorption removal effect of Sb(III). Therefore, pH is one of the most important parameters affecting the Sb(III) ion adsorption process [21]. In this study, the best adsorption effect has been achieved at pH = 2.

Effect of Dosage

Fig. 3 shows the variations of Sb(III) removal rate under different dosages of FTHSA. The removal rate of Sb(III) increased linearly to 93.2% with the dosage increasing from 1000 mg L^{-1} to 4800 mg L^{-1}, and slowly increased to 96.0% with the dosage increasing to 5600 mg L^{-1}. This indicates that the removal rate is not significantly elevated when the dosage of FTHSA is over 4800 mg L^{-1}. This was absolutely consistent with other observations by Sun, et al. [22-23]. It was reported that the adsorbent surface provided more functional groups and adsorption sites with the increasing dosage, and the removal rate increased. On the other hand, the removal rate is to remain within a stable range and is no longer elevated when desorption has achieved dynamic equilibrium. So, taking into account costs and removal efficiency, the best dosage of FTHSA should be 4800 mg L^{-1}.

Effects of Initial Concentration

As Shown in Fig. 4, excellent Sb(III) removal was achieved when the initial concentration of Sb(III) is within 5~50 mg L^{-1}, with the removal efficiency between 99.0% to 97.5%. Moreover, the concentration of Sb(III) in solution is below 0.05 mg L^{-1}. However,

the removal efficiency decreased from 87.1% to 34.4% when the initial concentration of Sb(III) increased from 75 mg L^{-1} to 450 mg L^{-1}. The removal efficiency decreased obviously. We deduced that FTHSA is well-suited for treatment of low antimony wastewater in the range of 0~50mg L^{-1}.

Effect of Temperature

As shown in Fig. 5, the removal rate of FTHSA for Sb(III) ions decreased with the increasing temperature. Removal rate of FTHSA for Sb(III) ions at 283.15, 293.15, and 303.15 K were found to be 95.3%, 93.3%, and 91.6%, respectively. The results showed that removal efficiency was slightly decreased with the increasing temperature. So the temperature has little impact on the removal of
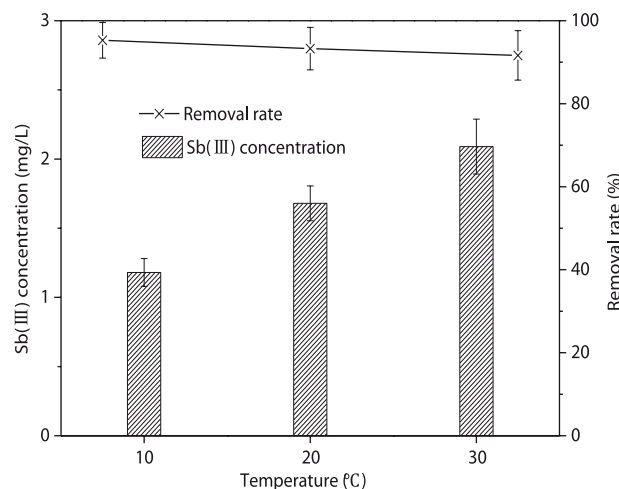

Fig. 5. Effects of temperature on the removal rate of Sb(III) ions by FTHSA: contact time = 120 min, pH = 2, dosage of sorbent = 4.2 g L^{-1}, volume of solution = 250 mL, initial concentration of Sb(III) = 25 mg L^{-1}

Sb(III) from aqueous solution onto FTHSA. Fan et al. [24] got the same results when they treated the antimony wastewater by other sorbents. Moreover, the changing trend of removal efficiency under different temperatures implied that adsorbent of Sb(III) from aqueous solution onto FTHSA belongs to exothermic reaction.

Adsorption Isotherm

In this study, the adsorption isotherm study was carried out using Langmuir, Freundlich, and Dubinin-Radushkevich (D–R) isotherm [25]. The applicability of the isotherm models to the adsorption study data was compared by judging the correlation coefficient (R^2) value [25].

Langmuir Isotherm Model

The Langmuir adsorption isothermal model describes a valid monolayer adsorption process, which assumes that all the adsorption sites have equal solute affinity and that adsorption at one site does not affect the adsorption at adsorbed molecules or an adjacent site [25]. It is expressed as follows:

$$q_e = \frac{q_{max} b C_e}{(1 + b C_e)} \tag{1}$$

...where q_e (mg g^{-1}) is the amount of the Sb(III) in solid phase, q_{max} (mg g^{-1}) is the maximum adsorption capacity, b(L mg^{-1}) is the Langmuir equilibrium constant (the greater the value, the stronger the adsorption performance of the adsorbent), and C_e (mg L^{-1}) is the equilibrium concentration of Sb(III) in the solution.

The linear plot of C_e/q_e vs. C_e is shown in Fig. 1a). The values of the constants q_{max} and b are listed in Table 1. The q_{max} values of 9.433 mg g^{-1} reflected that the maximum adsorption amount of FTHSA is bigger than cyanobacteria (4.88 mg g^{-1}) [10], seaweed (4.0 mg g^{-1}) [11], but is much smaller than Lichens (81.1 mg g^{-1}) [9]. The b values of 0.119 L mg^{-1} reflected that the adsorption performance is stronger than Fe(III)-treated fungi aerobic granules (0.112 L mg^{-1}) [26], and weaker than ferric hydroxide (0.275 L mg^{-1}) [27]. In all, FTHSA has a high adsorption amount.

Freundlich Isotherm Model

The Freundlich adsorption isothermal model is applicable to both monolayer reversible adsorption and multilayer adsorption. It is given as Eq. (2).

$$q_e = K_f C_e^{1/n} \tag{2}$$

... where C_e is the equilibrium concentration of Sb(III) in solution (mg L^{-1}), and K_f and $1/n$ are the Freundlich isotherm parameters that describe adsorption capacity and adsorption intensity, respectively.
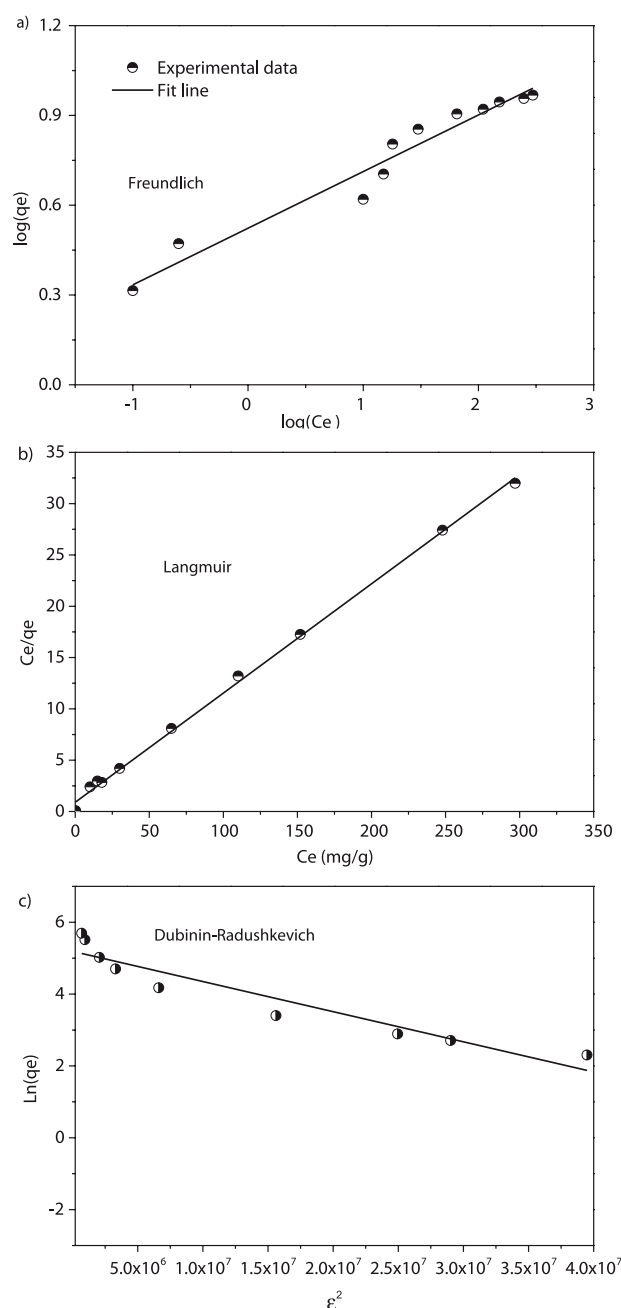

Fig. 6. Plots of adsorption isotherm model for the equilibrium date of Sb(III) adsorption onto FTHSA at 20ºC: a) Langmuir, b) Freundlich, and c) D-R isotherms.

The values of K_f and $1/n$ can be determined experimentally by plotting log q_e versus log C_e. As shown in Table 1, K_f and $1/n$ were 3.336 and 0.189, respectively. The values of $1/n$ are much smaller than 0.5, implying a close relation between adsorbate and adsorbent. It is concluded that the adsorbate can be easily adsorbed when the value of $1/n$ is between 0.1 and 0.5, while it is difficult to be adsorbed when the value of $1/n$ is over 2.0 [28]. The value of R^2 ($R^2 > 0.96$), Freundlich models were fit well the adsorption of Sb(III), which implied that there was both electrostatic interaction and ion exchange during the adsorption process. SEM characterization also

Table 1. Isotherm parameters for the adsorption of Sb(III) onto FTHSA.

Models	Langmuir	Freundlich	D-R
Parameters	q_{max}=9.433 mg g^{-1}	K_f= 3.336	β= -8.39E^{-8} mol^2/KJ^2
	b = 0.119 L mg^{-1}	$1/n$ = 0.189	q_s = 179.45 mg g^{-1}
	--	--	E = 24.1 mol KJ^{-1}
	R^2 = 0.9977	R^2 = 0.9636	R^2 = 0.8940

further confirmed that these materials had a larger hole volume size and smaller aperture.

Dubinin-Radushkevich Model

The D-R isotherm model is more widely used than the Langmuir isotherm or Freundlich isothermal, because it does not assume a homogeneous surface or constant adsorption potential [25]. It may be expressed as:

$$Ln(q_e) = Ln(q_s) - \beta\varepsilon^2 \quad (3)$$

…where β is the D-R isotherm constant (mol^2 kJ^{-2}), q_s is the theoretical isotherm saturation capacity (mg g^{-1}), and ε is the Polanyi potential – calculated as follows:

$$\varepsilon = RTln(1 + 1/C_e) \quad (4)$$

…where R is universal gas constant, 8.314 Jmol^{-1}K^{-1}; T is the absolute temperature (293.15K); and C_e (mol L^{-1}) is the concentration of Sb(III) in equilibrium solution.

The experimental data of D-R model had been analyzed by linear method from the plot of lnq_e vs. ε^2. As shown in Fig. 6c) and Table 1, the plot of lnq_e vs. ε^2 gives a straight line with the R^2 of 0.8940, and the values of q_s and β are 8.39E^{-8} mol^2 KJ^{-2} and 179.45 mg g^{-1}, respectively, which are determined from the intercept and slope using the linear regression method. Parameter β offers noteworthy information about the mean adsorption energy, which is the free energy change when one mole of ion is transferred to the surface of the sorbents from the solution [29]. It is calculated by Eq. (5):

$$E = (-2\beta)^{-1/2} \quad (5)$$

The value of E is useful for estimating the type of adsorption process [28]. According to the nature of the forces existing between the adsorbate and sorbent, the adsorption process can be classified as physical adsorption (1-8 KJ mol^{-1}), ion exchange (9-16 KJ mol^{-1}), and chemical adsorption (>16KJ mol^{-1}) [30]. The value of E in this study was found to be 24.1 mol KJ^{-1} (Table 1), indicating that the adsorption mechanism of Sb(III) onto FTHSA is chemical adsorption [29-30].

In conclusion, Langmuir isotherm parameters fit quite well with the experimental data for Sb(III) adsorption on FTHSA and yielded isotherms that agreed well with the observed behavior (R^2>0.99), indicating a monolayer adsorption process [28]. The adsorption capacity of Sb(III) on FTHSA at 293.15 K from Langmuir model was 9.433 mg g^{-1}. D-R isotherm further supported that the adsorption Sb(III) on FTHSA was a chemical sorption process.

Adsorption Kinetics

As everyone knows, adsorption kinetics are dominated by physical and chemical characteristics of the adsorbent during the mass migration process [31]. In order to investigate the kinetic characteristics of the adsorption process of Sb(III) ions onto FTHSA from aqueous solution, pseudo first-order, pseudosecond-order, Elovich [32], and intraparticle diffusion [31] kinetic models are used to fit the experimental data.

Pseudo First-Order Model

The pseudo first-order equation based on solid adsorption capacity is the most common and may be written as Eq. (6) [32]:

$$q_t = q_e(1 - \exp(-k_1 t)) \quad (6)$$

…where k_1(min^{-1}) is the pseudo first-order adsorption rate constant, and q_t and q_e (mg g^{-1}) are the adsorption capacities at time t (min) and at equilibrium, respectively.

As shown in Fig. 7a) and Table 2, the plot fitted the experimental data, and the calculated value of q_e (9.340 mg g^{-1}) is very consistent with the experimental value of q_e (9.433 mg g^{-1}). So it implies that the adsorption process of Sb(III) ions onto FTHSA can well be described by the pseudo first-order model.

Pseudo Second-Order Model

The pseudo second-order kinetic model assumes that the adsorption rate is controlled by the chemical adsorption mechanism, which involves electron sharing or electron transfer between the adsorbent and the adsorbate. It is described as Eq. (7).

$$q_t = q_e - q_e / (k_2 q_e t + 1) \quad (7)$$

Table 2. Calculated kinetic parameters for the adsorption of Sb(III) onto FTHSA.

Models	Pseudo first -order model	Pseudo second -order model	Elovich model	Intraparticle diffusion model	
Equation	$q_t = q_e(1-exp(-k_1t))$	$q_t= q_e -(q_e/(k_2q_et+1)$	$q_t = ln(\beta\alpha)/\beta+(1/\beta)lnt$	$q_t = \alpha_i+k_{4i}t^{0.5}$	
Parameters	q_e= 9.340mg g^{-1}	q_e =10.185mg g^{-1}	α = 2.026 mg mg^{-1} min^{-1}	α_1 = 0.381 mg g^{-1}	α_2 = 8.595 mg g^{-1}
	k_1 = 0.0616min^{-1}	k_2 = -0.088g mg^{-1} min^{-1}	β = 0.883g mg^{-1}	k_{41} = 1.262mg.g^{-1}.min$^{-0.5}$	k_{42} = 0..058 mg.g^{-1}. min$^{-0.5}$
	R^2= 0.992	R^2 = 0.993	R^2= 0.872	R^2_1 = 0.972	R^2_2 = 0.923

...where k_2 (g mg^{-1} min^{-1}) is the pseudo second-order adsorption rate constant, and q_e and q_t (mg g^{-1}) are Sb(III) adsorption capacity at equilibrium and at time t (min), respectively.

The fitting curve of q_t vs. t is plotted in Fig. 7a) and is used to obtain the calculated pseudo second-order parameters and correlation coefficient. The values of theoretical q_e (10.185 mg g^{-1}, Table 2) and experimental q_e (9.433 mg g^{-1}) are approximately equal to each other, and the correlation coefficient (R^2) is up to 0.993, which reveals the adsorption of Sb(III) ions onto FTHSA following the pseudo second-order kinetic model [25, 28].

Elovich Model

The Elovich model primary has been used to describe the kinetics of the chemisorption of gases on solids. But the same researchers applied this model to describe chemisorption of adsorbate by a solid in an aqueous medium. This model is formulated with Eq. (8):

$$q_t = \ln(\alpha\beta)/\beta+(1/\beta)\ln t \tag{8}$$

...where q_t (mg g^{-1}) is Sb(III) adsorption capacity at time t (min), α (mg mg^{-1} min^{-1}) is the sorption constant for Sb(III), and β (g mg^{-1}) is related to surface coverage and chemical activation energy.

As seen from the Fig. 7c), the fitting curve does not converge well when the Elovich model was applied to the experimental data. But the sorption of Sb(III) onto FTHSA are examples of heterogeneous systems because the reactions involve component types that exhibit different chemisorption activation energies [25, 28].

Intraparticle Diffusion model

The intraparticle diffusion model describes the mechanism of diffusion between particles and the pores of the adsorbent. It is expressed with Eq. (9):

$$q_t = a_i + k_{4i}t^{0.5} \tag{9}$$

...where k_{4i} (mg.g^{-1} min$^{-0.5}$) is a rate constant of stage i, which is related to the thickness of the boundary layer, and α_i (mg g^{-1}) is an intraparticle diffusion model constant of stage i. Adsorption capacity q_t versus $t^{0.5}$ should be linear.

If the plot passes through the origin, the rate-limiting process may be from intraparticle diffusion. However, if the data presents multi-linear plots, two or more steps are contained in the adsorption process.

As seen from Fig. 7b), adsorption capacity q_t vs. $t^{0.5}$ shows two stages that are strongly linear but different slopes. The first stage described the rapid external resistance to mass transfer surrounding the surface of adsorption particles. The second stage represented the
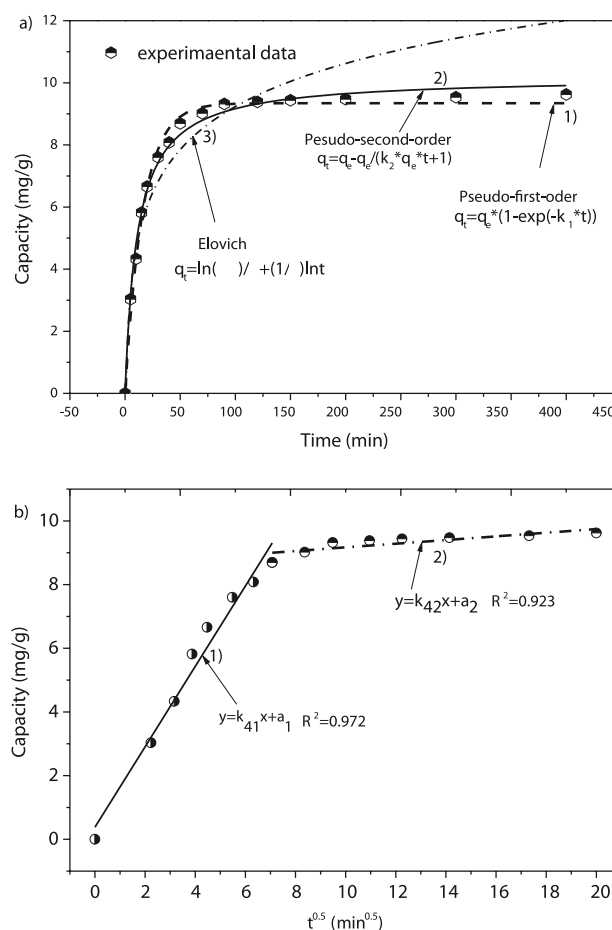

Fig. 7. Plots of pseudo first-order a), pseudo second-order b), Elovich c), and intra-particle diffusion d) models for the kinetic data of Sb(III) adsorption onto FTHSA: contact time = 120 min, pH = 2, dosage of adsorbent = 4.2 g L^{-1}, volume of solution = 250 mL, initial concentration of Sb(III) = 25 mg L^{-1}, temperature = 30°C.

gradual absorption stage with the intraparticle diffusion dominating. The calculated intercept (α_1, α_2) value are 0.381 and 8.595, respectively, suggesting that the pore diffusion was not the sole rate-controlling step due to the difference in rate of mass transfer in the first and second stages of adsorption. These findings implied that the rate-dominating step of the adsorption process of Sb(III) onto FTHSA might be originated from boundary layer diffusion or external mass transfer effects [25, 28].

Comparing the results obtained from the above four models, the pseudo second-order model can best fit with

FTHSA adsorption on Sb(III). The whole adsorption process of Sb(III) adsorption onto FTHSA was in conformity with the pseudo second-order kinetic model. It is possible to announce that the chemical adsorption on FTHSA surface plays a dominant role in the adsorption process [33], and that Sb(III) ions can combine with thiol groups of FTHSA through covalent chemical bonds.

Adsorption Mechanisms

Morphology

As shown in Fig. 8a), the morphology of humus sludge adsorbent was heterogeneous with few small bulges on the surface with EDS analysis. It contained C, O, Al, Si, Ca, Cl, K, and Fe (Table 3), and Sb iron was not detected. After Fe(III) treatment, as expected, many pores were seen on the FTHSA surface (Fig. 8b), and the contents of Fe were 5.66 wt.%, 8.2 times compared to the humus sludge adsorbent. Similar results also were found by Wang et al. [12] and M.J. Jimenez-Cedillo, et al. [34]. Moreover, the content of K was much smaller than before treatment, which implied that the K^+ was important for the modification of humus sludge adsorbent with an ion exchange effect [12]. After adsorption of Sb(III), the Sb content in FTHSA increased to 1.32 wt.%, which implied that Sb(III) ions were adsorbed onto it.

The FT-IR spectra of the humus sludge adsorbent, FTHSA, and after sorption of Sb(III) are presented in Fig. 9. As shown in Fig. 9a), broad strong absorption bands observed at 3423 cm^{-1} corresponded to O-H stretching vibration of the hydroxyl groups from the alcohols, and carboxylic acids or N-H stretching vibration. Four peaks at 2958, 2925, 2854, and 1401 cm^{-1} displayed the asymmetric stretching vibration, symmetric stretching vibration, bending vibration, and symmetric bending vibration of -CH$_2$ The bends at 1654 and 1538 cm^{-1} display the -C=O and C-N stretching vibrations of amide I from peptide bonds in proteins and C-N stretching vibration and N-H deformation vibration of amide II from peptide bonds in proteins, respectively [12]. A weak band observed at 1079 cm^{-1} was C-O stretching vibration and attributed to the presence of the alcohols or carboxylic acids [34]. The big peaks observed at 1036 cm^{-1} was O-H stretching vibrations and were attributed to the presence of lots of polysaccharides [12]. Bands less than 1000 cm^{-1} are fingerprint spectrum, which provided the information of phosphoric acid group and sulfur-containing group [35].

The obvious changes of FTHSA in the FT-IR spectra were presented in Fig. 9b). FTHSA displayed a broader peak in the range of 3414 cm^{-1}, which implied the presence of O-H and N-H functional groups on the surface. The bands in the range of 2960-2852 cm^{-1} were owed to the C-H stretching vibration, which shifted in FTHSA. The peak at 1654 cm^{-1}, which was assigned to the C=O stretching vibration for the amide I band from EPS [36], moved to 1650 cm^{-1} in FTHSA. The band at 1036 cm^{-1} also shifted to 1040 cm^{-1} owing to the O-H
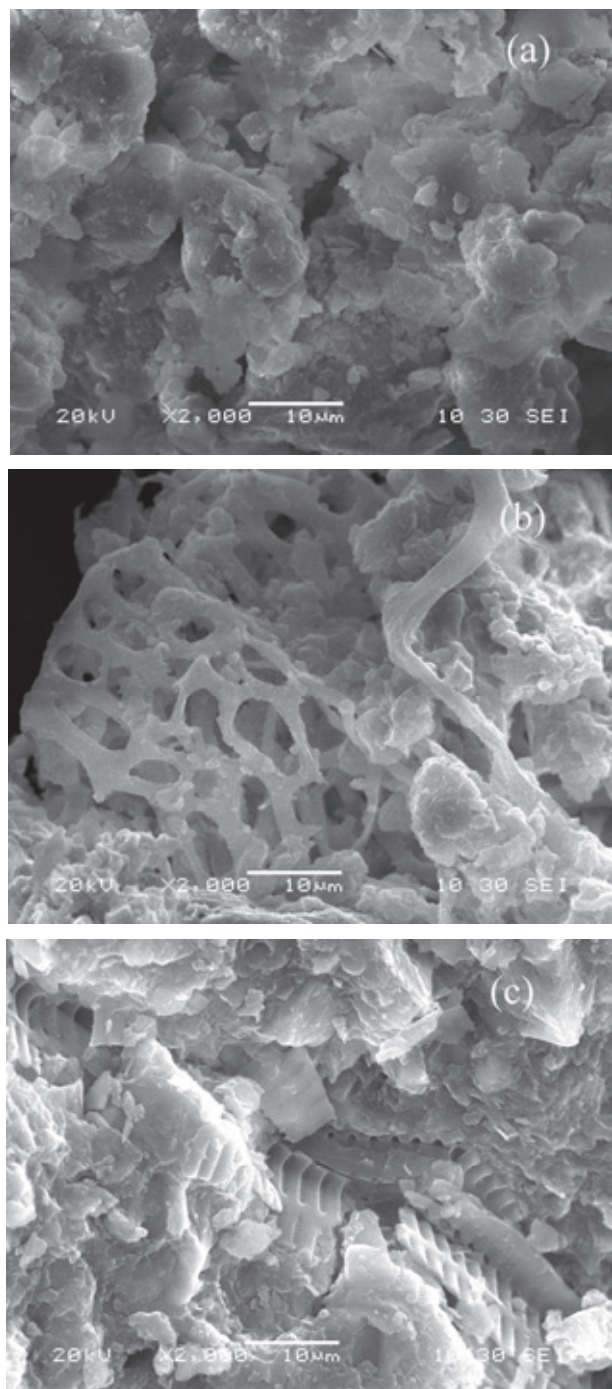

Fig. 8. SEM images of humus sludge sorbent derivatives: a) humus sludge sorbent, b) FTHSA, c) FTHSA with Sb(III).

Table 3. Elemental composition of humus sludge sorbent, FTHSA, and FTHSA with Sb(III).

Element		C K	O K	Al K	Si K	Ca K	Cl K	K K	Fe L	Sb L	Total
Composition (Wt.%)	Humus sludge sorbent	32.68	17.98	9.85	16.82	4.41	13.45	4.12	0.69	--	100
	FTHSA	32.52	17.03	9.41	16.81	4.03	13.74	0.8	5.66	--	100
	FTHSA with Sb(III)	32.47	17.05	8.93	15.82	4.45	14.05	1.12	4.79	1.32	100

stretching vibrations from polysaccharide, which implied that the polysaccharide played an important role in Fe-treatment [12].

These results suggest that the functional groups were successfully changed by the Fe(III)-treatment. After the adsorption of Sb(III), FTHSA FT-IR spectra also changed significantly (Fig. 8c), with characteristic peak position changing to 3403, 2926, 1648, 1546, 1039, and 534 cm^{-1}. The peaks in the range of 3400-3430 cm^{-1} are due to the stretching vibrations of N-H and O-H bonds [36-37]. The movement of the absorption peak at 1648 cm^{-1} is assigned to the C=O stretching vibration for the amide I band [36]. The weak peak at 1401 cm^{-1} corresponds to the C-O stretching vibration in the phenolic hydroxyl groups and anti-symmetry stretching of COO. The strong peak at 1040 cm^{-1} is attributed to the C–O stretching vibration. The movement of that position indicates that the C–O bond from the humus reacts with the Sb(III). Additionally, the wave peak shifted from 536 to 534, which is ascribed to the stretching vibration of the Sb(III)-O [27]. These results indicate that the chemical interactions as ion exchange among the metal ions and N-H, O-H, C=O, COO, and C-O were mainly involved in the adsorption.

Conclusions

Adsorption behavior and mechanism of Sb(III) onto FTHSA surface under different conditions have been investigated. The adsorption of Sb(III) onto FTHSA were
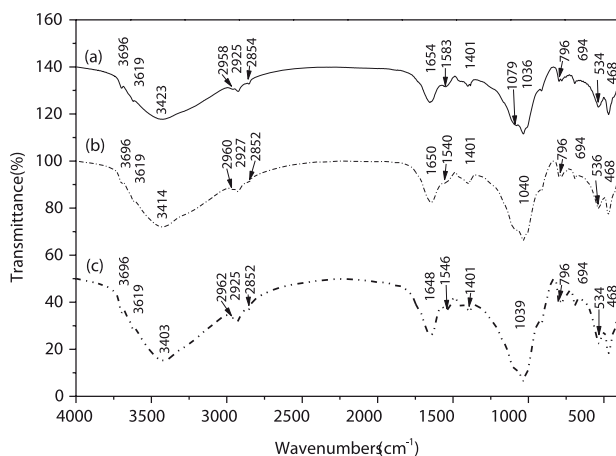
affected by dosage, contact time, initial concentration of Sb(III), and pH. And the value of maximum adsorption capacity of FTHSA was obtained as 9.433 mg/g. The Langmuir model plot was the best fit to the experimental data of Sb(III) ions adsorption. The pseudo second-order model can best fit with FTHSA adsorption of Sb(III). This also suggested that the chemical adsorption on FTHSA surface played a dominant role in the adsorption process. The chemical interactions as ion exchange among the metal ions and N-H, O-H, C=O, COO, and C-O were mainly involved in the adsorption of Sb(III) onto FTHSA. The FTHSA may be an efficient and cheap sorbent for removal the Sb(III) from wastewater.

Acknowledgements

References

1. JOHNSON C.A., MOENCH H., WERSIN P., KUGLER P., WENGER C. Solubility of antimony and other elements in samples taken from shooting ranges. Environmental Quality, **12** (34), 248, **2005**.

2. NING Z.P., XIAO T.F. Supergene geochemical behavior and environmental risk of antimony. Earth and Environment, **35** (2), 176, **2004**.

3. WU F.C., ZHENG J., PAN X.L., LI W. Prospect on Biogeochemical cycle and Environmental effect of antimony. Advances in Earth Science, **23** (4), 350-, **2008**.

4. UNGUREANU G., SANTOS S., BOAVENTURA R., BOTELHO C. Arsenic and antimony in water and wastewater: overview of removal techniques with special reference to latest advances in adsorption. Journal of Environmental Management, **151** (1), 326, **2015**.

5. INDIKA HERATH, METHTHIKA VITHANAGE, JOCHEN BUNDSCHUH Antimony as a global dilemma: Geochemistry, mobility, fate and transport. Environmental Pollution, **223**, 545, **2017**.

6. KANG M., KAMEI T., MAGARA Y. Comparing polyaluminum chloride and ferric chloride for antimony removal. Water Research, **37** (17), 4171, **2003**.

7. ZHU J., WU F.C. Application of Modified Fly Ash in Treatment of Antimony Mineral Processing Wastewater. Journal of Environmental Science, **30** (2), 361, **2010**.

8. ZHANG YAN, PANG ZHIHUA, LEI YUTAO Study on Influencing Factors and Kinetics of Antimony Ion

Fig. 9. FT-IR spectra of: a) humus sludge sorbent, b) FTHSA, c) FTHSA with Sb(III).

Treatment by Coagulation and Sedimentation. Journal of Safety and Environment, **13** (3), 50-53, **2013**.

9. ULUOZLU O.D., SARI A., TUZEN M. Biosorption of antimony from aqueous solution by lichen (Physcia tribacia) biomass. Chemical Engineering Journal, **163** (3), 382, **2010**.

10. WU F., SUN F., WU S., YAN Y., XING B. Removal of antimony(III) from aqueous solution by freshwater cyanobacteria Microcystis biomass. Chemical Engineering Journal, **183**, 172, **2012**.

11. UNGUREANU G., SANTOS S.C.R., VOLF I., BOAVENTURA R.A.R., BOTELHO C.M.S. Biosorption of antimony oxyanions by brown seaweeds: Batch and column studies. Journal of Environmental Chemical Engineering, **5** (4), 3463, **2017**.

12. LI WANG, CHUNLI WAN, DUU-JONG LEE, XIANG LIU, YI ZHANG, CHEN X.F., JOO-HWATAY Biosorption of antimony (V) onto Fe(III)-treated aerobic granules. Bioresource Technology, **158** (2), 351, **2014**.

13. CHUNLI WAN, LI WANG, DUU-JONG LEE, QINLAN ZHANG, JIENI LI, XIANG LIU Fungi aerobic granules and use of Fe(III)-treated granules for biosorption of Sb5+. Journal of the Taiwan Institute of Chemical Engineers, **45**, 2610, **2014**.

14. WANG XIAONING, ZHU NANWEN, YIN BINGKUI Preparation of sludge-based activated carbon and its application in dye wastewater treatment. Journal of Hazardous Materials, **153** (1/2), 227, **2008**.

15. XIANG W.Y., ZHANG Z.M. Preparation of composite adsorbent with chitosan and activated sludge. Acta Scientiae Circumstantiae, **34** (11), 2792, **2014**.

16. XUEHUA LI, XIAOMIN DOU, JUNQING LI Antimony(V) removal from water by iron-zirconium bimetal oxide:Performance and mechanism. Journal of Environmental Science, **24** (7), 1197, **2012**.

17. ESPEN MARIUSSEN, IDA VAA JOHNSEN, STRØMSENG A.E. Selective adsorption of lead, copper and antimony in runoff waterfrom a small arms shooting range with a combination of charcoal and iron hydroxide. Journal of Environmental Management, **150**, 281, **2015**.

18. JIMÉNEZ-CEDILLO M.J., OLGUÍN M.T., FALL C., COLIN-CRUZ A. As(III) and As(V) sorption on iron-modified non-pyrolyzed and pyrolyzed biomass from Petroselinum crispum (parsley). Journal of Environmental Management, **117**, 242, **2013**.

19. KUMAR B.B., MOUE J., KAWAKITA HBK BISWAS, INOUE K. Effective removal and recovery of antimony using metal-loaded saponified orange waste. Hazardous Materials, **172** (2-3), 721, **2009**.

20. WATKINS R., WEISS D., DUBBIN W., PEEL K., COLES B., ARNOLD T. Investigations into the kinetics and thermodynamics of Sb(III) adsorption on goethite (α-FeOOH). Colloid Interface Science, **303**, 639, **2006**.

21. XUEHUA LI, XIAOMIN DOU, JUNQING LI Antimony(V) removal from water by iron-zirconium bimetal oxide:Performance and mechanism. ScienceDirect, **24** (7), 1197, **2012**.

22. SUN F.H., HU X.W., GUO F., WU F.C. Biosorption of Sb (III) by Microcystis Aerosol Additive. Environmental Science Research, **29** (12), 1849, **2016**.

23. SUN F., SUN W.L. Biosorption behavior and mechanism of beryllium from aqueous solution by aerobic granule. Chemical Engineering Journal, **172** (2), 783, **2011**.

24. HONG-TAO FAN, WEN SUN, BING JIANG, QING-JIE WANG, DA-WU LI, CONG-CONG HUANG, KANG-JUN Z.Z.A.W., WANG A. Adsorption of antimony(III) from aqueous solution by mercaptofunctionalized silica-supported organic-inorganic hybrid sorbent:Mechanism insights. Chemical Engineering Journal, **286**, 128, **2016**.

25. FAN H.T., SUN W., JIANG B., WANG Q.J., LI D.W. dsorption of antimony(III) from aqueous solution by mercaptofunctionalized silica-supported organic-inorganic hybrid sorbent:Mechanism insights. Chemical Engineering Journal, **286**, 128, **2016**.

26. WAN C., WANG L., LEE D.J., ZHANG Q., LI J. Fungi aerobic granules and use of Fe(III)-treated granules for biosorption of Sb5+. Journal of the Taiwan Institute of Chemical Engineers, **45**, 2610, **2014**.

27. XU W., WANG H., LIU R., ZHAO X., QU J. The mechanism of antimony(III) removal and its reactions on the surfaces of Fe-Mn binanr oxide. Joumal of colloid and interface science, **363** (1), 320, **2011**.

28. ZHAO Z., WANG X., ZHAO C., ZHU X., DU S. Adsorption and desorption of antimony acetate on sodium montmorillonite. Colloid Interface Science, **345**, 154, **2010**.

29. ZHENG H., WANG Y., ZHENG Y., ZHANG H., LIANG S., LONG M. Equilibrium, kinetic and thermodynamic studies on the sorption of 4-hydroxyphenol on Crbentonite. Chemical Engineering Journal, **143** (117-123), 1173, **2008**.

30. VASILIU S., BUNIA I., RACOVITA S., NEAGU V. Adsorption of cefotaxime sodium salt on polymer coated ion exchange resin microparticles: kinetics equilibrium and thermodynamic shudyies. carbohydr .Polym, **85**, 376, **2011**.

31. NAIYA T.K., BHATTACHARYA A.K., DAS S.K. Adsorption of Cd(II) and Pb(II) from aqueous solutions on activated alumina. Colloid Interfaces Sci, **333**, 14, **2009**.

32. LAGERGREN S. About the theory of so-called adsorption of soluble substances. Kungliga Svenska Vetensk. Handl, **24**, 1, **1898**.

33. WANG J.J., LI X.N. Ion-imprinted composite hydrogels with excellent mechanical strength for selective and fast removal of Cu^{2+}. Ind. Eng. Chem.Res., **52**, 572, **2013**.

34. JIMÉNEZ-CEDILLO M.J,. OLGUÍN M.T, FALL C., COLIN-CRUZ A. As(III) and As(V) sorption on iron-modified non-pyrolyzed and pyrolyzed biomass from Petroselinum crispum (parsley). Journal of Environmental Management, **117**, 242, **2013**.

35. XU H., LIU Y. Mechanisms of Cd^{2+}, Cu^{2+} and Ni^{2+} biosorption by aerobic granules [J] Separation and purification technology., **58** (3), 400, **2008**.

36. PRADHAN S., SINGH S., RAI L.C. Characterization of various functional groups present in the capsule of Microcystis and study of their role in biosorption of Fe, Ni and Cr, Bioresour. Technol., **98**, 595, **2007**.

37. DAS S.K., DAS A.R., GUHA A.K. A study on the adsorption mechanism of mercury on Aspergillus versicolor biomass. Environment Science Technology, **41**, 8281, **2007**.